Cancer Chemother Pharmacol (2013) 71:133–143
DOI 10.1007/s00280-012-1988-6

ORIGINAL ARTICLE

PK-PD modeling of combination efficacy effect from administration of the MEK inhibitor GDC-0973 and PI3K inhibitor GDC-0941 in A2058 xenografts

Edna F. Choo · Chee M. Ng · Leanne Berry · Marcia Belvin · Nicholas Lewin-Koh · Mark Merchant · Laurent Salphati

Received: 2 April 2012 / Accepted: 18 September 2012 / Published online: 7 October 2012

Abstract
Purpose Mutations and activations of the MEK and PI3K pathways are associated with the development of many cancers. GDC-0973 and GDC-0941 are inhibitors of MEK and PI3K, respectively, currently being evaluated clinically in combination as anti-cancer treatment. The objective of these studies was to characterize the relationship between the plasma concentrations of GDC-0973 and GDC-0941 administered in combination and efficacy in A2058 melanoma xenograft.
Methods GDC-0973 and GDC-0941 were administered to A2058 tumor-bearing mice daily (QD) or every third day (Q3D) either as single agents or in combination. A semi-mechanistic population anti-cancer model was developed to simultaneously describe the tumor growth following QD/Q3D single-agent and QD combination treatments. The interaction terms ψ included in the model were used to assess whether the combination was additive. Using this model, data from the Q3D combination regimen were simulated and compared with the observed tumor volumes.
Results The model consisting of saturable tumor growth provided the best fit of the data. The estimates for ψ were not significantly different from 1, suggesting an additive effect of GDC-0973 and GDC-0941 on tumor growth inhibition. The population rate constants associated with tumor growth inhibition for GDC-0973 and GDC-0941 were 0.00102 and 0000651 μM^{-1} h^{-1}, respectively. Using the model based on single-agent and QD combination efficacy data, simulations adequately described the tumor growth from the Q3D combination regimen.
Conclusions These findings suggest that, based on minimal data, it is possible to predict the effects of various combinations preclinically and also assess the potential clinical efficacy of combinations using human pharmacokinetic inputs.

Keywords MEK inhibitor · PI3K inhibitor · Pharmacokinetic–pharmacodynamic modeling · Tumor xenograft · A2058 tumor

Electronic supplementary material The online version of this article (doi:10.1007/s00280-012-1988-6) contains supplementary material, which is available to authorized users.

E. F. Choo · L. Salphati (✉)
Drug Metabolism and Pharmacokinetics, Genentech, Inc., 1 DNA Way, South San Francisco, CA 94080, USA
e-mail: salphati.laurent@gene.com

C. M. Ng
School of Medicine, University of Pennsylvania, Clinical Pharmacology and Therapeutics, Children Hospital of Philadelphia, Philadelphia, PA 19104, USA

L. Berry · M. Belvin · M. Merchant
Cancer Signaling and Translational Oncology, Genentech, Inc., 1 DNA Way, South San Francisco, CA 94080, USA

N. Lewin-Koh
Nonclinical Biostatistics, Genentech, Inc., 1 DNA Way, South San Francisco, CA 94080, USA

Introduction

Combining multiple targeted anti-cancer agents with the goal of providing effective therapy has been increasingly explored in oncology. Many cancers (e.g., melanoma, colorectal, pancreatic, ovarian, NSCLC, and thyroid cancers) have a high and overlapping frequency of oncogenic mutations as well as other genomic alterations that activate both RAS and PI3K pathways. In tumor cells, inhibition of

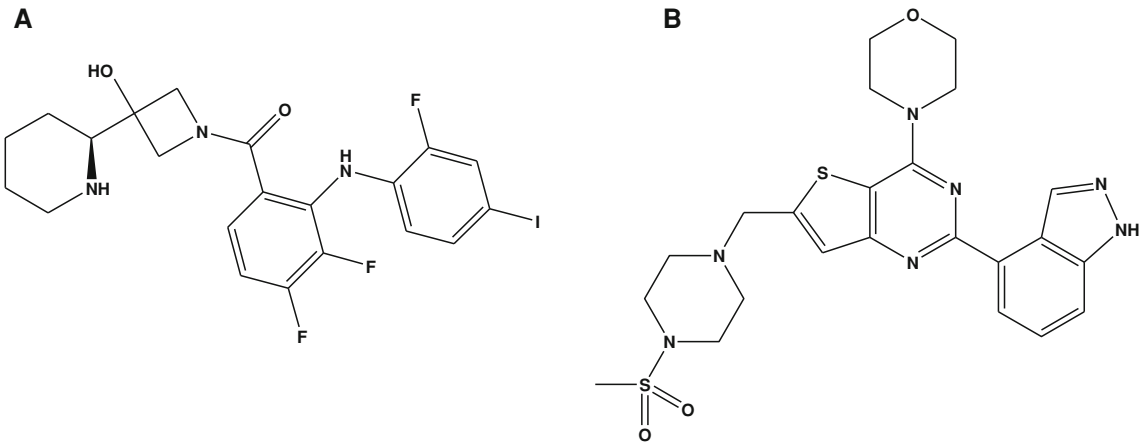

Fig. 1 Chemical structure of GDC-0973 (**a**) and GDC-0941 (**b**)

either the MEK or PI3K pathway can result in activation of the other through feedback [30]; therefore, inhibition of both pathways represents a promising anti-cancer strategy. This is evidenced by improved in vitro potency and in vivo efficacy observed from combined PI3K and MEK inhibition in preclinical efficacy models [5, 14].

The RAS/RAF/MEK/ERK signaling pathway is involved in cellular responses relevant to tumorigenesis, including cell proliferation, invasion, survival and angiogenesis. This pathway is activated by a diverse array of growth factors, cytokines and proto-oncogenes, which transduce their growth-promoting signals through the activation of the small G protein RAS. Activation of RAS leads to the activation of RAF followed by the activation of MEK, which then phosphorylates and activates ERK [10, 17, 28, 29, 38]. GDC-0973 ([3,4-Difluoro-2-(2-fluoro-4-iodo-phenylamino)-phenyl]-((*S*)-3-hydroxy-3-piperidin-2-yl-azetidin-1-yl)-methanone) (Fig 1a) is a MEK1/2 inhibitor. It is potent and selective in biochemical and cell-based assays with an IC_{50} estimate of 0.004 μM against the purified MEK1 enzyme, a cellular pERK IC_{50} of 0.009 μM in the HCT116 cell line and an IC_{50} of 6.9 μM against A2058 cell proliferation. It also has broad in vivo efficacy in xenograft models with BRAF and KRAS mutations [13].

The phosphoinositide 3-kinase (PI3K) signaling pathway, a parallel pathway to MEK, is a major downstream effector of receptor tyrosine kinases, such as human epidermal growth factor-2 (HER2), epidermal growth factor receptor (EGFR) and insulin-like growth factor-1 receptor that stimulates cell proliferation, promotes survival and inhibits apoptosis. Abnormal regulation of this central signaling pathway has been identified in a large number of cancer types and occurs through various mechanisms [1, 2, 4, 8, 16, 19, 25, 31].

GDC-0941 (2-(1*H*-Indazol-4-yl)-6-(4-methanesulfo-nyl-piperazin-1-ylmethyl)-4-morpholin-4-yl-thieno[3,2-*d*] pyrimidine) (Fig. 1b) is a novel small molecule inhibitor of the PI3K pathway currently being evaluated in phase II studies as an anti-cancer agent [26]. It is selective for the class I (α, *β*, *δ*, *γ*) PI3K [9] and is efficacious against the U87MG glioblastoma and IGROV-1 human ovarian cancer xenograft models in athymic mice [22]. GDC-0941 is considered an inhibitor of class I PI3K isoforms with IC_{50} of 0.003, 0.033, 0.003 and 0.075 μM against p110α, *β*, *δ* and *γ*, respectively. It potently inhibits the phosphorylation of downstream Akt in PC3-NCI (prostate) and MCF7.1 cells (breast), with IC_{50} ranging from 0.028 to 0.037 μM. It is also able to inhibit the proliferation of MCF7.1, PC3-NCI and A2058 cells with $IC_{50's}$ of 0.72 μM, 0.28 μM and 2.1 μM, respectively [9, 13].

Currently, GDC-0973 and GDC-0941 are being administered as single agents and in combination in cancer patients (www.clinicaltrials.gov). However, prior to clinical combination trials, initial proof-of-concept studies were conducted using mouse xenograft models.

These investigations in preclinical models provided useful information when comparing efficacy from administration of a single compound to efficacy observed following co-administration of two compounds. In mouse models, factorial combinations that would not be acceptable in human subjects can be explored to better understand the drug interaction profile in vivo. To inform clinical studies, it is often useful to determine the target exposure/dose associated with efficacy and the regimen that maximizes the efficacy of single or combination therapy. However, direct extrapolation of exposure from mouse to human may be confounded by differences in the pharmacokinetics between mouse and human. Therefore, to further leverage the xenograft efficacy data, pharmacokinetic–pharmacodynamic (PK-PD) modeling and simulations were conducted. The objectives of the present studies were to characterize the efficacy of the combination of

GDC-0973 and GDC-0941 in vivo, develop a PK-PD model describing the relationship between the plasma concentrations of both agents and A2058 tumor growth inhibition, and verify that the model could be utilized to predict efficacy for different dosing regimens with minimal xenograft efficacy data.

Materials and methods

Chemicals

GDC-0973 and GDC-0941 were provided by Genentech Inc (South San Francisco, USA). Solvents used for analysis were of analytical or HPLC grade (Fisher Scientific, Pittsburgh, PA, USA). All other reagents or material used in this study were purchased from Sigma-Aldrich (St Louis, MO, USA) unless otherwise stated. The Genentech Institutional Animal Care and Use Committee approved all procedures in animals.

Pharmacokinetic studies in mouse

Female athymic nu/nu mice weighing 25–28 g (Charles River Laboratories, Hollister, CA, USA) were administered oral doses of 3, 10 or 30 mg/kg GDC-0973 in 0.5 % methylcellulose/0.2 % Tween 80 (MCT). The pharmacokinetics of GDC-0941 in nu/nu mouse was previously described [24]. The pharmacokinetics of GDC-0973 (3 mg/kg) and GDC-0941 (100 mg/kg) was also evaluated when dosed in combination. Blood samples ($\sim$1 mL) from these studies were collected at 0.083, 0.25, 0.5, 1, 2, 4, 8 and 24 h post-dose via cardiac puncture (terminal collection) into tubes containing potassium ethylenediaminetetraacetic acid (K_2EDTA) anti-coagulant. Immediately upon collection, the blood was mixed with K_2EDTA and stored on ice. Within 30 min, blood samples were centrifuged at approximately 1,000–1,500$\times g$ for 5 min at 4 °C, and plasma was harvested. Plasma samples were stored at −80 °C until analysis.

Samples were prepared for analysis by placing a 25 μL aliquot into a 96-well plate followed by the addition of 25 μL of internal standard and 200 μL acetonitrile. After the samples were vortexed and centrifuged for 5 min at 3,400 rpm, 50 μL of the supernatant was diluted with 350 μL of water, of which 20 μL was injected onto the column. Concentrations of GDC-0973 in plasma were determined by a LC/MS/MS assay using a Sciex API 3,000 triple quadrupole mass spectrometer (Applied Biosystems, Foster City, CA, USA) connected with a CTC HTS PAL autosampler (LEAP Technologies, Chapel Hill, NC). Chromatographic separation was achieved with gradient elution on an ACE 5 phenyl column (100 × 2.1 mm, 5 μm) (MAC-MOD Analytical, Chadds Ford, CA, USA) at room temperature and a pair of Shimadzu LC-10AD pumps with a SCL-10A controller (Shimadzu, Columbia, MD, USA). The aqueous mobile phase was water with 0.1 % formic acid, and the organic mobile phase was acetonitrile with 0.1 % formic acid. The gradient elution was run at 0.500 mL/min flow rate from 20 to 80 % organic in 1 min with the total run time of 5 min. Ionization was conducted in the positive ion mode at an ionspray interface temperature of 450° C, using nitrogen nebulizing and heating gas. GDC-0973 and the internal standard (^{13}C-stable label) were analyzed in the MRM mode using the transitions m/z 532.1 → 249.1 and 401.2 → 322.2, respectively. Calibration curve, which ranged from 0.005 to 10 μM for GDC-0973, was fit to a $1/x^2$ weighted quadratic regression model. The concentration of GDC-0973 samples was determined by interpolation from the standard curve. A run was deemed acceptable when quality control (QC) samples were ±25 % of the nominal concentration, except the lowest QC where ±30 % was accepted. The dynamic range of the GDC-0973 and GDC-0941 assays was 0.005–10 μM.

Xenograft efficacy studies

All procedures involving animals were performed in accordance with Genentech's Institutional Animal Care and Use Committee guidelines. To generate tumors, A2058 cells (ATCC, Manassas, VA, USA) were harvested in the log phase of growth and resuspended in 50 % Matrigel matrix (BC Biosciences, Bedford, MA, USA) in phosphate-buffered saline at a concentration of 5×10^7 cells/mL. Each 9–10-week-old female athymic nude mice (Harlan, Sommerville, NJ, USA) included in the study received a subcutaneous injection of 1×10^7 A2058 cells (0.2 mL cell suspension) into the right flank. Tumor volume (TV) was calculated from diameters using the formula:

$$\text{TV } (\text{mm}^3) = a \times b^2 \times 0.5,$$

where a and b are the shortest and longest perpendicular tumor diameters, respectively.

Tumor volumes and body weights were measured at least twice weekly until the end of the study. Mice were euthanized if their tumor volume exceeded 2,000 mm^3 and/or if their body weight dropped by more than 20 %. GDC-0973, GDC-0941 or the vehicle (control) were administered orally by gavage in a volume of 200 μL once tumor volumes reached 100–300 mm^3 (8–10 days post inoculation). Treatment groups ($n = 7$ mice per group) received oral doses of GDC-0973 and GDC-0941, as a single agent or as combinations either on a daily (QD) or on a once-every-third-day (Q3D) regimen for 20 or 21 days. The treatment groups in the xenograft efficacy experiments included in this study were as follows:

Experiment 1
Single agent
GDC-0973—vehicle, 1, 6 and 10 mg/kg once QD
GDC-0941—vehicle, 10, 30 and 100 mg/kg QD
Combination
GDC-0973 1 mg/kg QD + GDC-0941—10, 30 and 100 mg/kg QD
GDC-0973 6 mg/kg QD + GDC-0941—10, 30 and 100 mg/kg QD
GDC-0973 10 mg/kg QD + GDC-0941—10, 30 and 100 mg/kg QD
Experiment 2
Single agent
GDC-0973—vehicle, 10, 15 and 20 mg/kg Q3D
GDC-0941—vehicle, 50, 100 and 150 mg/kg Q3D
Combinations
GDC-0973 10 mg/kg Q3D + GDC-0941—50, 100 and 150 mg/kg Q3D
GDC-0973 15 mg/kg Q3D + GDC-0941—50, 100 and 150 mg/kg Q3D
GDC-0973 20 mg/kg Q3D + GDC-0941—50, 100 and 150 mg/kg Q3D

Preclinical pharmacokinetics

Mouse PK parameters of GDC-0973 and GDC-0941 were obtained by fitting the PK model to mean concentration–time profiles of the compounds using SAAM II (Saam Institute, University of Washington, Seattle, WA, USA). The PK data of GDC-0973 and GDC-0941 were described by a one-compartment model with linear absorption and elimination according to the following:

$$\mathrm{Ct} = \frac{\mathrm{Ka} \times \mathrm{Dose}}{(\mathrm{Ka} - \mathrm{Ke}) \times V/F} \times (\mathrm{e}^{-k \times t} - \mathrm{e}^{-\mathrm{Ka} \times t}) \quad (1)$$

where Ct represents the mean plasma concentrations, Ka is absorption rate constant, Ke is elimination rate constant and *V*/*F* is volume of distribution.

Pharmacokinetic–Pharmacodynamic (PK-PD) Modeling

A semi-mechanistic anti-cancer model was used to simultaneously describe the tumor growth data after vehicle, single-agent and combination administration of GDC-0973 and/or GDC-0941. The model was constructed to mimic the physiological process and consisted of linear or saturable tumor growth and drug response model. The differential equation describing the semi-mechanistic model is as follows:

$$\frac{\mathrm{d(TV)}}{\mathrm{d}t} = k_{\mathrm{ng}}(\mathrm{TV})(1 - \mathrm{TG}) - E_{0973} \times \psi_1 \times \mathrm{TV} - \mathrm{E}_{0941} \times \psi_2 \times \mathrm{TV} \quad (2)$$

TV (mm^3) is defined as the tumor volume and *t* (h) is time. TG is a tumor growth model, where TG = 0 for linear growth and $\mathrm{TG} = \mathrm{TV}/\mathrm{TV}_{\mathrm{max}}$ for logistic and saturable tumor growth where $\mathrm{TV}_{\mathrm{max}}$ is the maximum growth capacity of tumors. E_{0973} and E_{0941} are the linear or saturable drug response models that are used to describe the anti-tumor effect of GDC-0973 and GDC-0941, respectively (Eqs. 3 and 4).

Linear drug response model:

$$\mathrm{E}_{0973} = \mathrm{A}_{0973} \times \mathrm{C}_{0973} \text{ and } \mathrm{E}_{0941} = \mathrm{A}_{0941} \times \mathrm{C}_{0941} \quad (3)$$

Saturable drug response model:

$$\mathrm{E}_{0973} = \frac{\mathrm{E\,max}_{0973} \times \mathrm{C}_{0973}}{\mathrm{EC}_{50-0973} + \mathrm{C}_{0973}} \mathrm{E}_{0941} = \frac{\mathrm{E\,max}_{0941} \times \mathrm{C}_{0941}}{\mathrm{EC}_{50-0941} + \mathrm{C}_{0941}} \quad (4)$$

where A_{0973} and A_{0941} represent the linear tumor growth inhibition effect of GDC-0973 and GDC-0941, respectively. C_{0973} and C_{0941} (μM) are the plasma concentrations of GDC-0973 and GDC-0941, respectively. For the saturable drug response model, Emax_{0973} and Emax_{0941} represent the maximum tumor inhibition effects of GDC-0973 and GDC-0941, respectively. $\mathrm{EC}_{50\text{-}0973}$ and $\mathrm{EC}_{50\text{-}0941}$ correspond to the concentration at half-maximal tumor inhibition of GDC-0973 and GDC-0941, respectively. The terms ψ_1 and ψ_2 are the interaction terms that are used to determine the interaction of each agent on each other during co-administration of GDC-0973 and GDC-0941, respectively. This interaction term concept was previously described by Koch et al. [15]. The values of ψ_1 and ψ_2 describe "additive" anti-tumor effects of each agent on each other when they are not significantly different from 1, and ψ values significantly greater or less than 1 signify the "greater-than" (or "synergistic") or "less-than" (or "antagonistic") additive anti-tumor effect from co-administration of the two agents. Hence, these interaction terms can be used to indicate the nature and intensity of the drug interactions.

To analyze the pooled tumor growth data from different studies (single and combination treatments) and repeated measurement of tumor volumes from the same animals over time appropriately, a nonlinear-mixed effect modeling approach with the Monte Carlo parametric expectation maximization (MCPEM) method implemented in S-ADAPT program [3, 20] was used to obtain the population model parameters. This population modeling approach addresses both repeated measurements and modest dropouts due to any non-treatment-related death of animals before the end of study [21]. The inter-individual variability among the model parameters were assumed to be log-normally distributed. Intra-individual variability was modeled with proportional error according to the following equations:

$$y_{ij} = yp_{ij} + yp_{ij} \times \varepsilon_{ij} \quad (5)$$

where y_{ij} and yp_{ij} are the jth measured and model-predicted values, respectively, for the ith individual mice, and ε_{ij} denote the proportional residual intra-individual random errors distributed with zero means and variances σ^2. To discriminate between two nested population models, a difference in an objective function of greater than 3.84 (1 degree of freedom with χ^2 distribution), which corresponds to a significant level of $p < 0.05$ was used. AIC model selection criterion was used to discriminate non-nested population model.

To test the ability of the model to predict the tumor growth data from new combination regimens, only data from studies with a single-agent (QD and Q3D) and combination treatments with QD regimens were used to develop the population model. The final population model was then used to simulate the tumor growth data from combination treatments with the Q3D dosing regimen. The results from the simulated studies were compared with the observed data and used to provide evidence that the derived population model could be used to describe the observed data from studies with new dosage regimens.

Results

Preclinical pharmacokinetics

The mean plasma concentration–time plots of GDC-0973 in mice at doses of 3, 10 and 30 mg/kg are shown in Fig. 1a. The preclinical pharmacokinetic parameters of GDC-0973 were estimated as follows: Ka = 0.579 h^{-1}, Ke = 0.185 h^{-1} and V/F = 18.7 L/kg (Fig. 2a). The estimated parameters for GDC-0941 were previously described [24] and are as follows: Ka = 10.4 h^{-1}, Ke = 0.228 h^{-1} and V/F = 19.9 L/kg. These parameters were used to simulate GDC-0973 and GDC-0941 plasma concentrations when fitting the model to the tumor volume data from xenograft efficacy studies. The pharmacokinetics of either compound was unaffected by the co-administration of either agent (Fig. 2b).

Xenograft efficacy

Tumor growth curves following a range of GDC-0973 and GDC-0941 single-agent oral doses administered daily (QD) and every 3rd day (Q3D) in A2058 ($BRAF^{V600E}$, $PTEN^{null}$ melanoma) xenograft tumor -bearing mice are shown in Figs. 3a–b and 4c–d, respectively. Tumor growth curve following combination of varying doses of GDC-0973 and GDC-0941 are shown in Fig. 4a–f. Overall, as single agents, administration of GDC-0973 and GDC-0941 resulted in dose-dependent inhibition of tumor growth in A2058 xenografts. At the highest single-agent doses tested, GDC-0973 achieved tumor growth inhibition (TGI) of 73 % and 68 % when dosed QD and Q3D, respectively. GDC-0941, at the highest doses, achieved a TGI of ~69 % when dosed QD and 50 % when dosed Q3D. When dosed in combination, one partial response (20 mg/kg GDC-0973 and 100 mg/kg GDC-0941) and a complete response (10 mg/kg GDC-0973 and 150 mg/kg GDC-0941) were observed with the combination Q3D regimen.

Pharmacokinetic–pharmacodynamic (PK-PD) modeling

A semi-mechanistic population model was developed to describe the pooled tumor growth data after vehicle, single-agent and combination treatment with GDC-0973 and GDC-0941 in the xenograft mouse model. A total of 1201 tumor growth data from 161 animals were used to develop the final population model. Initially, the model with linear tumor growth and drug response model with no drug interaction, with the assumption of an additive effect (ψ_1 and ψ_2 were fixed to 1), was developed. The model, however, failed to describe the tumor growth data. Therefore, the model was modified by adding saturable tumor growth components while ψ_1 and ψ_2 were fixed to 1. As a result, the fit of this modified model to the data was markedly improved ($p < 0.05$). Further modification of the model with saturable drug response components (Eq. 4) did not significantly improve the model fit ($p > 0.05$), and the EC_{50} values for both drugs were poorly estimated (%SE >50). In addition, allowing the flexibility of the model to estimate the interaction terms ψ_1 and ψ_2 did not result in significant decrease in the objective function and improvement of model fit. Furthermore, the model estimates of the ψ_1 and ψ_2 did not significantly differ from 1, suggesting that the combination of GDC-0973 and GDC-0941 had additive effects on tumor growth inhibition in the xenograft mouse model. Therefore, the final population model consisted of saturable tumor growth, linear drug response and an additive effect for combination of GDC-0973 and GDC-0941 on tumor growth inhibition.

The final model reasonably predicted the observed tumor growth data after vehicle, single-agent and combination (QD) treatment of GDC-0973 and GDC-0941. Figure 5a shows individual predicted versus observed tumor volume data for all animals. Generally, there was good agreement between the predicted and observed individual data, and the diagnostic plots of the final model identified no systematic bias (Fig. 5b–d). Representative plots of observed and model-predicted tumor volume in four animals receiving vehicle, single-agent and combination treatments of GDC-0973 and GDC-0941 are shown in Supplemental Figure 1A–D. These plots further demonstrated that the final model reasonably described the observed data. The

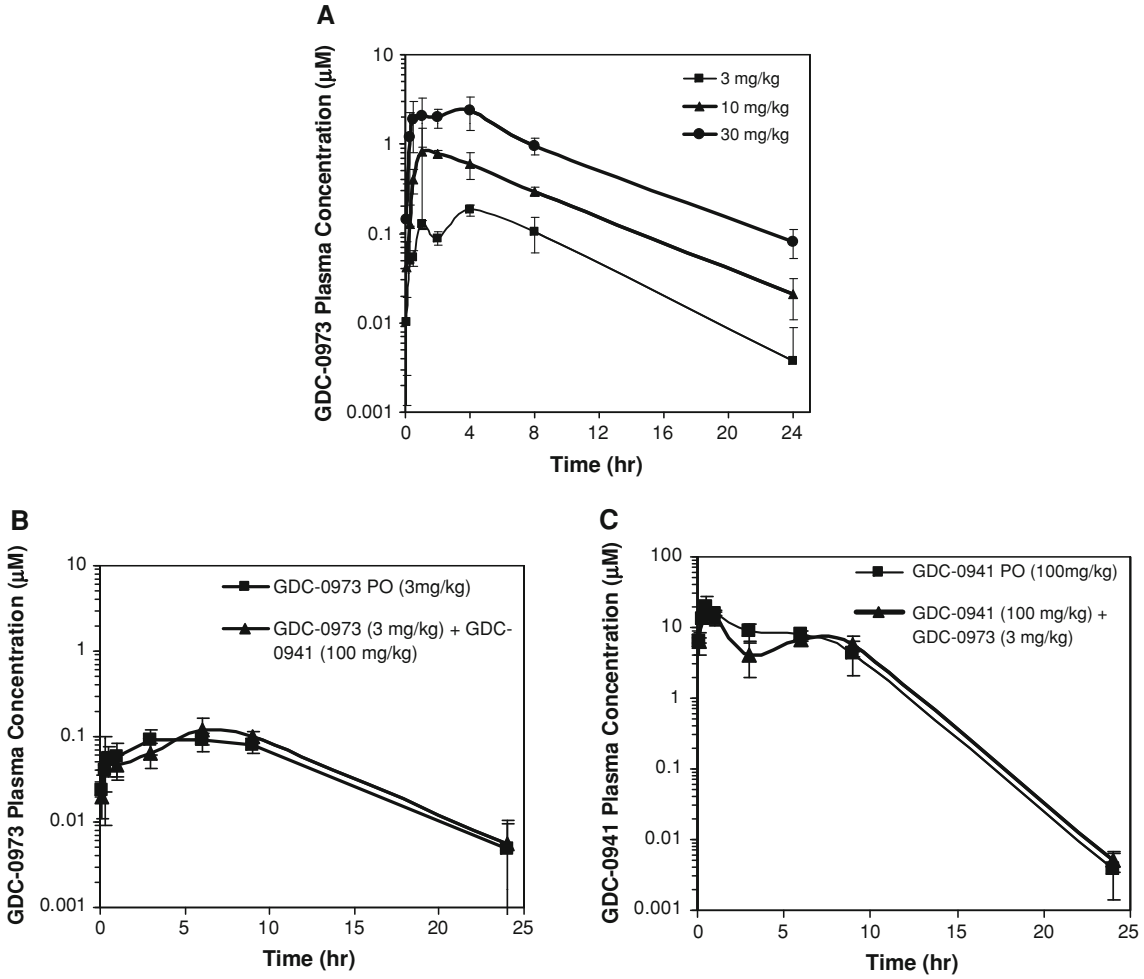

Fig. 2 Concentration–time plot of GDC-0973 in mice at doses of 3, 10 and 30 mg/kg (**a**). Concentration–time plot of GDC-0973 when administered alone and in combination with GDC-0941 (**b**) and when GDC-0941 was administered alone and in combination with GDC-0973 (**c**); the overlapping curves suggest that co-administration of either compound with the other does not alter its pharmacokinetics (presented as concentration ± SD; $n = 3$ per time point)

estimated final population model parameters are presented in Table 1. The population mean rate constant associated with tumor inhibition for GDC-0973 and GDC-0941 were 0.00102 and 0.00065 $\mu M^{-1}\ h^{-1}$, respectively. The population mean maximum growth capacity of tumors TV_{max} was 3947 mm^3. The final PK/PD and inter- and intra-subject variability parameters for GDC-0973 and GDC-0941 were estimated with good precision, with percent standard error of the parameter estimates <50 %.

This final population model was then used to simulate the tumor volume–time profile from animals that received different dosages and combination regimens not included in the dataset used for model development. These animals received different doses of GDC-0973 and GDC-0941 on Q3D regimens. The results from the simulated results were compared with the observed data (Supplemental Figure 2A–B). In general, the simulated results agreed with those observed in the study. This indicates that our understanding of the drug exposure and tumor response relationships was adequate and allowed us to predict the time course of tumor response after single-agent and combination treatment of GDC-0973 and GDC-0941 in the A2058 xenograft mouse model.

Discussion

PK-PD modeling and simulations have increasingly been incorporated into the drug discovery and development process [18]. Although the structure of the models utilized may vary, the overall goal of PK-PD modeling is to integrate information from various experiments to facilitate decision making, for example, dose/schedule selection and trial design. In oncology, xenograft tumor models

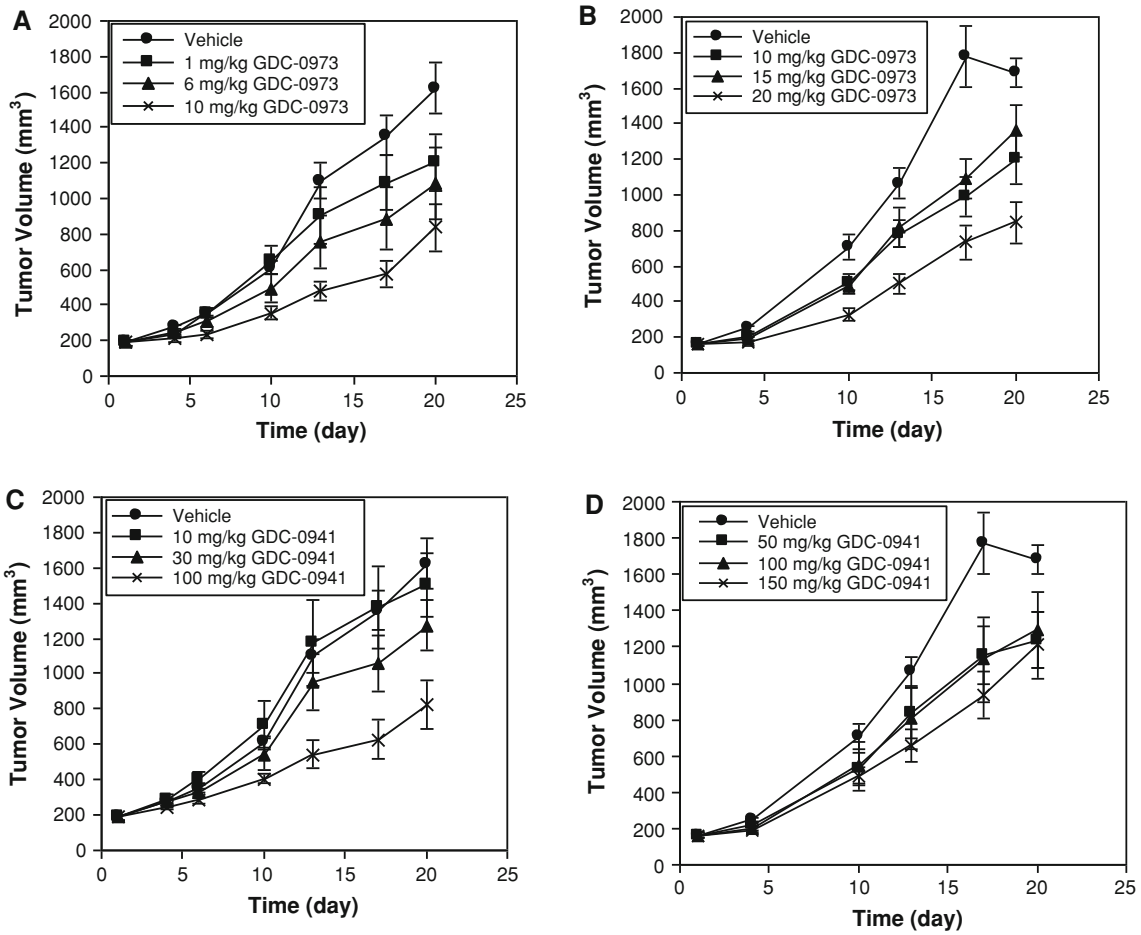

Fig. 3 Mean (±SEM; $n = 7$) tumor volume versus time plots after QD (**a**) Q3D (**b**) dosing of GDC-0973 as a single-agent and QD (**c**) and Q3D (**d**) dosing of GDC-0941 as a single agent

are the main pharmacology model used to evaluate New Molecular Entities (NME) [33]. The information from PK-PD modeling of mouse xenograft efficacy data has been useful in extrapolating data from mouse to humans [6, 11, 32, 34, 35]. To date, most of the data from PK-PD modeling has been from single-agent efficacy studies. However, cancer treatments are more frequently combined, usually with standard of care chemotherapy, but increasingly with other targeted agents to maximize efficacy and/or to avoid resistance by targeting parallel pathways. To support these clinical regimens, preclinical efficacy studies with combined agents are usually conducted. Several approaches can be used in analyzing the effects of combination, such as the Chou and Talalay combination index in vitro [6], and the isobologram method in vivo [12]. However, these approaches do not take into account inputs of dynamic changes in concentrations (i.e., pharmacokinetics), and as such, cannot be utilized to predict effects in human based on changes in the concentration–time profile.

As combined agents including combinations of 2 NME's are tested earlier in the drug development process, when optimal dosing regimens for either compound are yet to be determined, preclinical PK-PD modeling becomes even more important. Therefore, in order to utilize the preclinical efficacy data from administration of combined agents, PK-PD modeling has recently been applied to describe combination xenograft efficacy data [11, 15, 23]. For instance, Rocchetti et al. [23] described the modeling of efficacy data from combined agents based on additivity of the effects from each agent. However, these authors mainly assessed the adequacy of their model by testing the goodness of fit in a study that included only 4 groups. Goteti et al. [11] proposed a similar model to predict tumor growth, assuming synergy between AZD7762 (a checkpoint kinase inhibitor) and irinotecan. In addition, they modified their model to interrogate the optimal dosing interval of two agents, AZD7762 and flavopiridol. The doses and interval predicted for the optimal efficacy of irinotecan in combination with AZD7762 and flavopiridol

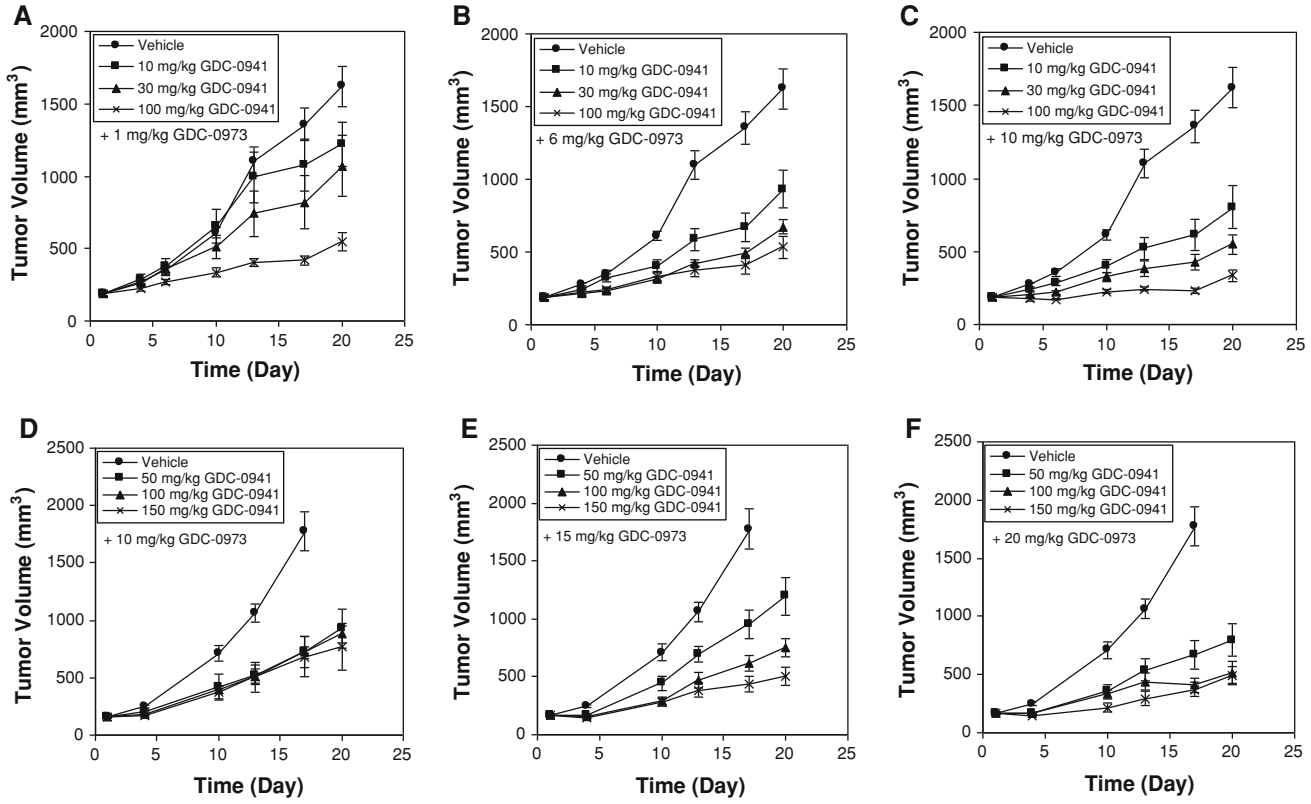

Fig. 4 Xenograft efficacy data (mean tumor volume ± SEM; $n = 7$) after QD administration of 1 mg/kg (**a**), 6 mg/kg (**b**) and 10 mg/kg (**c**) of GDC-0973 in combination with 10, 30 and 100 mg/kg QD of GDC-0941 (*top panel*). Xenograft efficacy data (mean tumor volume ± SEM; $n = 7$) after Q3D administration of 10 mg/kg (**d**), 15 mg/kg (**e**) and 20 mg/kg (**f**) of GDC-0973 in combination with 50, 100 and 150 mg/kg Q3D of GDC-0941 (*bottom panel*)

based on their modeling appeared to be consistent with the reported effective clinical doses and schedules, respectively [11]. In these examples, the potency of each individual compound on tumor growth was initially determined and then fixed when modeling combination efficacy data.

The modeling approach proposed here to describe the combination effect of GDC-0973 and GDC-0941 was a logical extension of the indirect response models that have been used to characterize single-agent xenograft efficacy data from a number of kinase inhibitors [24, 36]. The population model was developed by simultaneously fitting the model to the majority of tumor volume versus time data from single-agent and combination treatments. The approach is similar to the model described by Koch et al. [15], where a multiplicative "interaction factor" was included in the equation to assess the nature and intensity of the interaction between the two drugs. However, rather than assuming that one agent affects the other, and not vice versa, we have incorporated an interaction factor, associated with each agent, assuming that efficacy of *each* compound could be contributing to a "less-than" or "greater-than" additive effect. In addition, the population modeling approach utilized in the study allows us to obtain reliable model parameter estimates from combining the data from different studies.

Although "additive" models have been previously proposed [11, 15, 23], this study is, to our knowledge, the first application of such a model to a large dataset and study design. Based on the model and simulations, the "additivity" of tumor growth inhibition from each agent in A2058 xenografts holds up across the range of doses tested, as well as different regimens that is, Q3D. While this model is specific in describing the in vivo effects of GDC-0973 and GDC-0941 on A2058 xenograft tumors, we have found that it also applies to other tumors (DLD-1; colorectal cancer $KRAS^{G13D}$) [13] for this combination. In the case of the dataset with A2058 xenografts, using the "additive" model described the combination effect of GDC-0973 and GDC-0941 adequately. This is consistent with the lack of pharmacokinetic interaction when these two compounds are co-administered and the biological activity of both compounds on parallel pathways, as described in detail by Hoeflich et al. [13].

Once established, such a model can be applied to describe and simulate combination efficacy using different dosing regimens (e.g., once every 2 days) without the need

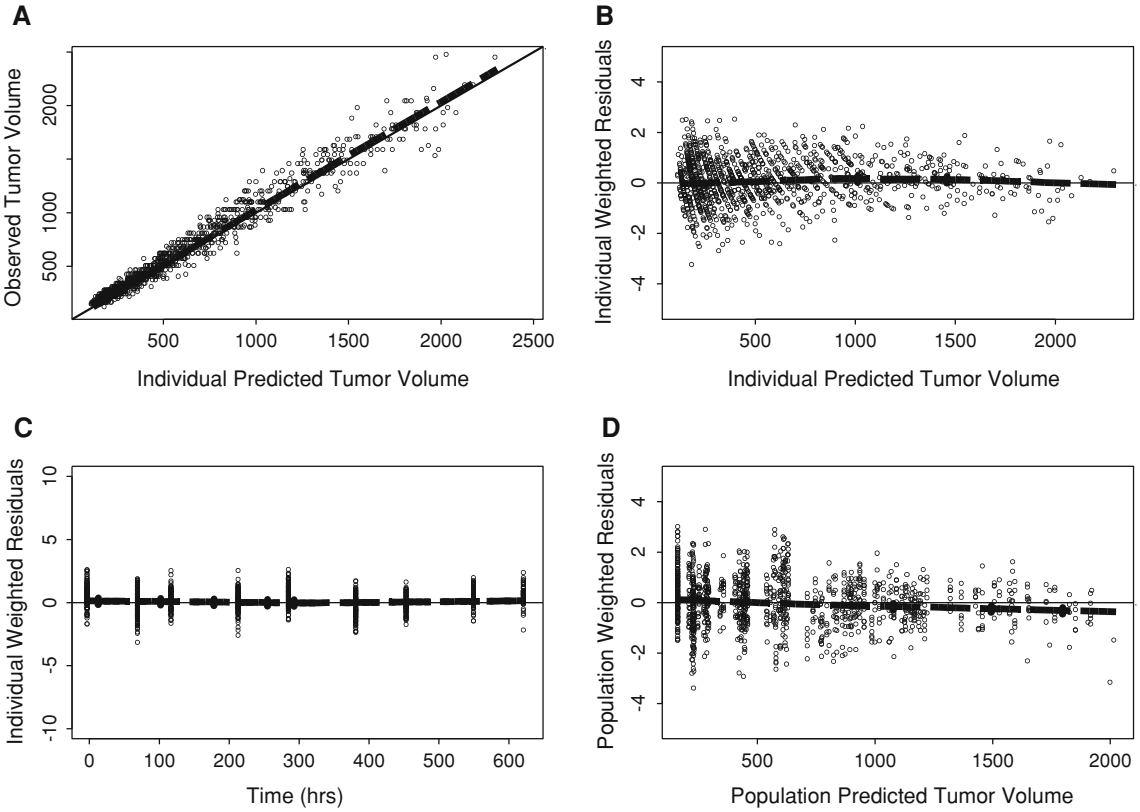

Fig. 5 Model diagnostic plots. Individual predicted versus observed tumor volume data (**a**). Individual weighted residual versus individual predicted tumor volume (**b**). Individual weighted residual versus time (**c**) and population conditional weighted residuals versus population predicted tumor volume (**d**); *Dotted line*, LOESS smoothing (*solid line*)

Table 1 Final population model parameters

Parameter	Population mean (%SE)[a]	Inter-individual variability (%SE)
Kng (h^{-1})	0.0544 (21.7)	0.100 (15.5)
A_{0973} (μM^{-1} h^{-1})	0.00102 (42.5)	0.670 (48.6)
A_{0941} (μM^{-1} h^{-1})	0.000651 (17.3)	0.217 (31.9)
V_{max} (mm^3)	3947 (7.2)	0.111 (22.7)
Ψ_1^b	1 (Fixed)	–
Ψ_2^b	1 (Fixed)	–
σ^c	0.145 (2.4)	–

[a] Percent standard error of the parameter estimate = standard error of estimates/parameter estimates ×100 %

[b] Estimates of Ψ was not significantly different from 1 and therefore fixed in the final model

[c] Inter-individual variability

for further experimental data, thus saving time and expense. The overarching goal in setting up this model is to be able to apply it to the clinical situation and therefore guide the clinical study design. For instance, based on substitution of human pharmacokinetic parameters for mouse pharmacokinetic parameters, we can predict doses at which signs of efficacy can be expected or simulate and predict efficacy at tolerated clinical doses and regimens. The information from these simulations is particularly important for combinations of NME where limited knowledge of clinical efficacy is available. There are caveats to this modeling approach such as the assumption that the growth rate of xenografts is maintained from mouse to humans. However, despite the limitations, the xenograft models continue to be the mainstay of preclinical assessment of anti-tumor efficacy [7, 27] and utilizing the data in a more quantitative manner is beneficial. Recently, it has been shown by PK-PD modeling and simulation that anti-tumor activity of targeted agents in genotypic-appropriate murine subcutaneous tumor model correlated with clinical response [37].

The model described here is not intended to provide full mechanistic/biological information *per se*. However, the simplicity of this modeling approach means that one could generate similar information on combination agents from multiple tumor types representing different genotypes. These data will not only provide insight into the applicability of xenograft models in predicting clinical outcome but, collectively, this information would also be useful in guiding rational dosing regimens in the clinic as well as provide an assessment of target exposures that may be

required clinically. Finally, as PK-PD modeling and simulations become increasingly applied in the drug development process, it will be important to conduct retrospective analysis as clinical efficacy data become available in order to gain insights into model refinement and application.

References

1. Aoki M, Batista O, Bellacosa A, Tsichlis P, Vogt PK (1998) The akt kinase: molecular determinants of oncogenicity. Proc Natl Acad Sci USA 95:14950–14955
2. Bagci-Onder T, Wakimoto H, Anderegg M, Cameron C, Shah K (2011) A dual PI3K/mTOR inhibitor, PI-103, cooperates with stem cell-delivered TRAIL in experimental glioma models. Cancer Res 71:154–163
3. Bauer RJ, Guzy S (eds) (2004) Monte carlo parametric expectation maximization (MC-PEM) method for analyzing population pharmacokinetic/pharmacodynamic (PK/PD) data. Kluwer Academic Publishers, Boston
4. Bellacosa A, de Feo D, Godwin AK, Bell DW, Cheng JQ, Altomare DA, Wan M, Dubeau L, Scambia G, Masciullo V, Ferrandina G, Benedetti Panici P, Mancuso S, Neri G, Testa JR (1995) Molecular alterations of the AKT2 oncogene in ovarian and breast carcinomas. Int J Cancer 64:280–285
5. Belvin M, Berry L, Chan J, Otter Dd, Friedman L, Hoeflich K, Koeppen H, Merchant M, Orr C, Rice K (2010) Intermittent dosing of the MEK inhibitor, GDC-0973, and the PI3K inhibitor, GDC-0941, results in prolonged accumulation of Bim and causes strong tumor growth inhibition in vivo. 22nd EORTC—NCI–AACR Symposium on Molecular Targets and Cancer Therapeutics Programme and Abstract Book Berlin, Germany. p 48
6. Chou TC, Talalay P (1984) Quantitative analysis of dose-effect relationships: the combined effects of multiple drugs or enzyme inhibitors. Adv Enzyme Regul 22:27–55
7. Damia G, D'Incalci M (2009) Contemporary pre-clinical development of anticancer agents–what are the optimal preclinical models? Eur J Cancer 45:2768–2781
8. Edgar KA, Wallin JJ, Berry M, Lee LB, Prior WW, Sampath D, Friedman LS, Belvin M (2010) Isoform-specific phosphoinositide 3-kinase inhibitors exert distinct effects in solid tumors. Cancer Res 70:1164–1172
9. Folkes AJ, Ahmadi K, Alderton WK, Alix S, Baker SJ, Box G, Chuckowree IS, Clarke PA, Depledge P, Eccles SA, Friedman LS, Hayes A, Hancox TC, Kugendradas A, Lensun L, Moore P, Olivero AG, Pang J, Patel S, Pergl-Wilson GH, Raynaud FI, Robson A, Saghir N, Salphati L, Sohal S, Ultsch MH, Valenti M, Wallweber HJ, Wan NC, Wiesmann C, Workman P, Zhyvoloup A, Zvelebil MJ, Shuttleworth SJ (2008) The identification of 2-(1H-indazol-4-yl)-6-(4-methanesulfonyl-piperazin-1-ylmethyl)-4-morpholin -4-yl-thieno[3,2-d]pyrimidine (GDC-0941) as a potent, selective, orally bioavailable inhibitor of class I PI3 kinase for the treatment of cancer. J Med Chem 51:5522–5532
10. Gollob JA, Wilhelm S, Carter C, Kelley SL (2006) Role of Raf kinase in cancer: therapeutic potential of targeting the Raf/MEK/ERK signal transduction pathway. Semin Oncol 33:392–406
11. Goteti K, Garner CE, Utley L, Dai J, Ashwell S, Moustakas DT, Gonen M, Schwartz GK, Kern SE, Zabludoff S, Brassil PJ (2010) Preclinical pharmacokinetic/pharmacodynamic models to predict synergistic effects of co-administered anti-cancer agents. Cancer Chemother Pharmacol 66:245–254
12. Greco WR, Bravo G, Parsons JC (1995) The search for synergy: a critical review from a response surface perspective. Pharmacol Rev 47:331–385
13. Hoeflich KP, Merchant M, Orr C, Chan J, Den Otter D, Berry L, Kasman I, Koeppen H, Rice K, Yang NY, Engst S, Johnston S, Friedman LS, Belvin M (2012) Intermittent administration of MEK inhibitor GDC-0973 plus PI3K inhibitor GDC-0941 triggers robust apoptosis and tumor growth inhibition. Cancer Res 72:210–219
14. Hoeflich KP, O'Brien C, Boyd Z, Cavet G, Guerrero S, Jung K, Januario T, Savage H, Punnoose E, Truong T, Zhou W, Berry L, Murray L, Amler L, Belvin M, Friedman LS, Lackner MR (2009) In vivo antitumor activity of MEK and phosphatidylinositol 3-kinase inhibitors in basal-like breast cancer models. Clin Cancer Res 15:4649–4664
15. Koch G, Walz A, Lahu G, Schropp J (2009) Modeling of tumor growth and anticancer effects of combination therapy. J Pharmacokinet Pharmacodyn 36:179–197
16. Li J, Yen C, Liaw D, Podsypanina K, Bose S, Wang SI, Puc J, Miliaresis C, Rodgers L, McCombie R, Bigner SH, Giovanella BC, Ittmann M, Tycko B, Hibshoosh H, Wigler MH, Parsons R (1997) PTEN, a putative protein tyrosine phosphatase gene mutated in human brain, breast, and prostate cancer. Science 275:1943–1947
17. Madhunapantula SV, Robertson GP (2008) Is B-Raf a good therapeutic target for melanoma and other malignancies? Cancer Res 68:5–8
18. Mager DE, Woo S, Jusko WJ (2009) Scaling pharmacodynamics from in vitro and preclinical animal studies to humans. Drug Metab Pharmacokinet 24:16–24
19. Maira SM, Stauffer F, Brueggen J, Furet P, Schnell C, Fritsch C, Brachmann S, Chene P, De Pover A, Schoemaker K, Fabbro D, Gabriel D, Simonen M, Murphy L, Finan P, Sellers W, Garcia-Echeverria C (2008) Identification and characterization of NVP-BEZ235, a new orally available dual phosphatidylinositol 3-kinase/mammalian target of rapamycin inhibitor with potent in vivo antitumor activity. Mol Cancer Ther 7:1851–1863
20. Ng CM, Joshi A, Dedrick RL, Garovoy MR, Bauer RJ (2005) Pharmacokinetic-pharmacodynamic-efficacy analysis of efalizumab in patients with moderate to severe psoriasis. Pharm Res 22:1088–1100
21. Pinheiro J, Bates D, DebRoy S, Sarkar D, the R Core team (eds) (2009) nlme: linear and nonlinear mixed effects models. R package v. 3.1-93. http://cran.r-project.org/
22. Raynaud FI, Eccles SA, Patel S, Alix S, Box G, Chuckowree I, Folkes A, Gowan S, De Haven Brandon A, Di Stefano F, Hayes A, Henley AT, Lensun L, Pergl-Wilson G, Robson A, Saghir N, Zhyvoloup A, McDonald E, Sheldrake P, Shuttleworth S, Valenti M, Wan NC, Clarke PA, Workman P (2009) Biological properties of potent inhibitors of class I phosphatidylinositide 3-kinases: from PI-103 through PI-540, PI-620 to the oral agent GDC-0941. Mol Cancer Ther 8:1725–1738
23. Rocchetti M, Del Bene F, Germani M, Fiorentini F, Poggesi I, Pesenti E, Magni P, De Nicolao G (2009) Testing additivity of anticancer agents in pre-clinical studies: a PK/PD modelling approach. Eur J Cancer 45:3336–3346
24. Salphati L, Wong H, Belvin M, Bradford D, Edgar KA, Prior WW, Sampath D, Wallin JJ (2010) Pharmacokinetic-pharmacodynamic modeling of tumor growth inhibition and biomarker modulation by the novel phosphatidylinositol 3-kinase inhibitor GDC-0941. Drug Metab Dispos 38:1436–1442
25. Samuels Y, Wang Z, Bardelli A, Silliman N, Ptak J, Szabo S, Yan H, Gazdar A, Powell SM, Riggins GJ, Willson JK, Markowitz S, Kinzler KW, Vogelstein B, Velculescu VE (2004) High frequency of mutations of the PIK3CA gene in human cancers. Science 304:554

26. Sarker D, Reid AH, Yap TA, de Bono JS (2009) Targeting the PI3K/AKT pathway for the treatment of prostate cancer. Clinical cancer research : an official journal of the American Association for Cancer Research 15:4799–4805
27. Sausville EA, Burger AM (2006) Contributions of human tumor xenografts to anticancer drug development. Cancer Res 66: 3351–3354, discussion 3354
28. Schreck R, Rapp UR (2006) Raf kinases: Oncogenesis and drug discovery. Int J Cancer 119:2261–2271
29. Sebolt-Leopold JS, Herrera R (2004) Targeting the mitogen-activated protein kinase cascade to treat cancer. Nat Rev Cancer 4:937–947
30. Sos ML, Fischer S, Ullrich R, Peifer M, Heuckmann JM, Koker M, Heynck S, Stuckrath I, Weiss J, Fischer F, Michel K, Goel A, Regales L, Politi KA, Perera S, Getlik M, Heukamp LC, Ansen S, Zander T, Beroukhim R, Kashkar H, Shokat KM, Sellers WR, Rauh D, Orr C, Hoeflich KP, Friedman L, Wong KK, Pao W, Thomas RK (2009) Identifying genotype-dependent efficacy of single and combined PI3K- and MAPK-pathway inhibition in cancer. Proc Natl Acad Sci USA 106:18351–18356
31. Staal SP (1987) Molecular cloning of the akt oncogene and its human homologues AKT1 and AKT2: amplification of AKT1 in a primary human gastric adenocarcinoma. Proc Natl Acad Sci USA 84:5034–5037
32. Tanaka C, O'Reilly T, Kovarik JM, Shand N, Hazell K, Judson I, Raymond E, Zumstein-Mecker S, Stephan C, Boulay A, Hattenberger M, Thomas G, Lane HA (2008) Identifying optimal biologic doses of everolimus (RAD001) in patients with cancer based on the modeling of preclinical and clinical pharmacokinetic and pharmacodynamic data. J Clin Oncol 26:1596–1602
33. Teicher BA (2006) Tumor models for efficacy determination. Mol Cancer Ther 5:2435–2443
34. Wang S, Guo P, Wang X, Zhou Q, Gallo JM (2008) Preclinical pharmacokinetic/pharmacodynamic models of gefitinib and the design of equivalent dosing regimens in EGFR wild-type and mutant tumor models. Mol Cancer Ther 7:407–417
35. Wang S, Zhou Q, Gallo JM (2009) Demonstration of the equivalent pharmacokinetic/pharmacodynamic dosing strategy in a multiple-dose study of gefitinib. Mol Cancer Ther 8:1438–1447
36. Wong H, Belvin M, Herter S, Hoeflich KP, Murray LJ, Wong L, Choo EF (2009) Pharmacodynamics of 2-[4-[(1E)-1-(hydroxyimino)-2,3-dihydro-1H-inden-5-yl]-3-(pyridine-4-yl)-1 H-pyrazol-1-yl]ethan-1-ol (GDC-0879), a potent and selective B-Raf kinase inhibitor: understanding relationships between systemic concentrations, phosphorylated mitogen-activated protein kinase kinase 1 inhibition, and efficacy. J Pharmacol Exp Ther 329: 360–367
37. Wong H, Choo EF, Alicke B, Ding X, La H, McNamara E, Theil FP, Tibbitts J, Friedman LS, Hop CE, Gould SE (2012) Antitumor activity of targeted and cytotoxic agents in murine subcutaneous tumor models correlates with clinical response. Clin Cancer Res 18:3846–3855
38. Zebisch A, Troppmair J (2006) Back to the roots: the remarkable RAF oncogene story. Cell Mol Life Sci 63:1314–1330